

# Passive seismic multicomponent imaging using geometrical optics theory

Aleksandar Jeremic\*, Julia Kurpan, Michael Thornton, Peter Duncan, MicroSeismic Inc.

## SUMMARY

Here, a method of passive seismic imaging using multicomponent (3-C) data is presented. It is a Beamforming/Kirchhoff type migration, which is based upon the isotropic elastic wave equation within geometrical optics theory. To account for the effects of the source mechanism, polarity corrections are applied.

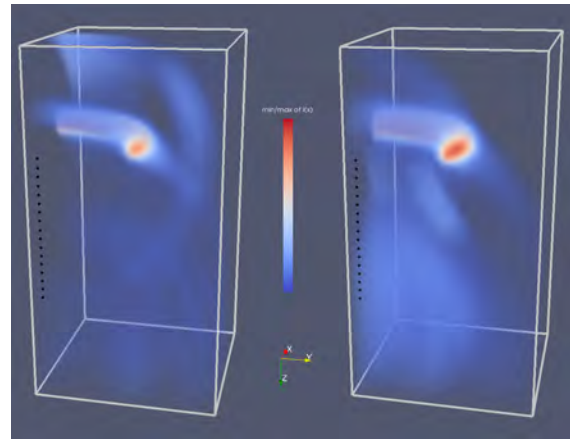
Mathematically, the goal in a passive seismic survey is to characterize the source term in elastic wave equation, given seismic velocities and measured displacements at some number of observation points. Following Haldorsen et al. (2013) approach, using Helmholtz decomposition (Muller, 2007), the source wavefield can be decomposed into a curl-free longitudinal component ( $L$ ) and divergence-free transverse ( $T$ ) components. They are utilized to locate and characterize the seismic event that sourced the wavefield. The method can be implemented for both surface and downhole receiver array geometries. Here we are presenting the method as it applies to downhole surveys. Both the synthetic and field data examples are demonstrated.

The synthetic example proves feasibility of the imaging technique, by producing the resulting image exactly in the place of the modeled synthetic event. We also confirm the accuracy of the approach with a real world example where the validity of the results are confirmed by quality-control of the steps of the imaging procedure, by the relative position to a treatment well of the event locations, and by the match of the imaged perforation shot to its known location.

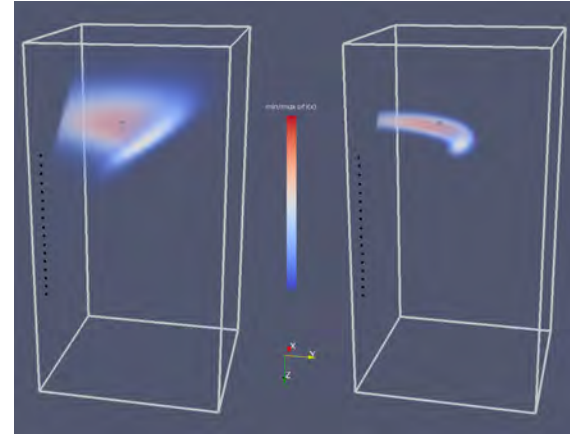
## INTRODUCTION

Passive seismic data recorded by surface arrays, which have large apertures, wide azimuths and high fold, are routinely used for imaging of microseismicity that occurs during hydraulic fracturing (Duncan and Eisner, 2010). Mapping of the microseismicity created during hydraulic fracturing, when tight shale formations are stimulated in order to increase permeability, is critical to understanding the well efficiency, to optimize completion processes and to maximize production. The method presented here can be used for 3-C data recorded both on/near Earth's surface and/or in downhole deployments to characterize and locate passive microseismic events. We present the theoretical basis, from which the 3-C imaging solution is derived. We then demonstrate the method using both synthetic and real field data

Historically, multicomponent data have been used for locating the passive seismic event. The most widely used method is the inversion of the picked first arrival of P and S waves (Geiger, 1912). This methodology is simple, straightforward, and computationally cheap. However, it is time consuming, tedious, and may contain a bias, based on the processor picking the arrival times. Instead, we are utilizing the full waveform



(a) Synthetic longitudinal -  $L$  (left) and transverse image -  $T$  (right) at origin time  $t_0$



(b) Synthetic stacked image at all times  $t_i$  (left) and the image at origin time  $t_0$  (right)

Figure 1: The synthetic passive seismic images with the source and receivers geometry

3-C imaging technique, which, in the past has typically been applied to surface array acquisition, for example, reverse-time type migration (Artman et al., 2010), applied only on surface geometries, and probabilistic non-linear inversion (Drew et al., 2005). The imaging procedure presented here is a modification of a commonly used method in earthquake seismology for wave-field propagation analysis, where if a location/back-azimuth of the seismic source is known, the 3-C data are rotated to so called radial, transverse and vertical components. The method is closest to Fuller et al. (2007) and Haldorsen et al. (2013) approaches. Comparing to the latter, the method uses the same concepts except the following:

- the imaging is done in the time domain
- the scaling of source wavefields is modified
- a moment tensor polarity correction is applied (Thornton and Eisner, 2011)

## Passive seismic multicomponent imaging using geometrical optics theory

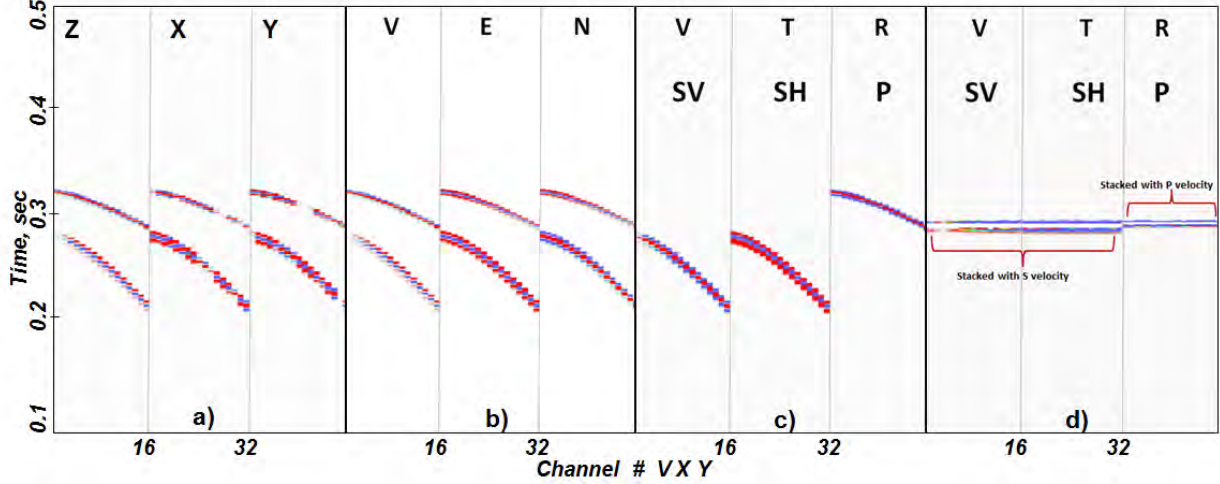


Figure 2: A half second time window of synthetic data on 16 levels 3-C geophones in the downhole monitoring well, sorted by components. a) raw data, b) oriented data to true/grid north, c) rotated data from known location to (R,T,V), and d) travel-time moveout applied data before the stacking procedure.

- the imaging condition is crosscorrelation of the RMS wavefields and,
- it is implemented as a fully 3-D approach, allowing for lateral changes in velocities.

### THEORY OF MULTICOMPONENT PASSIVE SEISMIC IMAGING - BASED ON GEOMETRICAL OPTICS

We start by noting that the displacement vector  $\mathbf{u}(\mathbf{x}, t)$  of an isotropic material body is governed by the elastic wave equation (note: vector quantities are presented in bold type, whereas scalars in normal type). The equation can be represented as a pair of acoustic wave equations (Shearer, 2009), that is, for a given density,  $\rho(\mathbf{x})$ , and P-wave and S-wave velocities,  $v_p(\mathbf{x})$  and  $v_s(\mathbf{x})$  respectively,

$$\frac{1}{v_p(\mathbf{x})^2} \frac{\partial^2 (\nabla \cdot \mathbf{u}(\mathbf{x}, t))}{\partial t^2} - \Delta (\nabla \cdot \mathbf{u}(\mathbf{x}, t)) = \frac{\nabla \cdot \mathbf{f}(\mathbf{x}, t)}{v_p(\mathbf{x})^2 \rho(\mathbf{x})} \quad (1)$$

$$\frac{1}{v_s(\mathbf{x})^2} \frac{\partial^2 (\nabla \times \mathbf{u}(\mathbf{x}, t))}{\partial t^2} - \Delta (\nabla \times \mathbf{u}(\mathbf{x}, t)) = \frac{\nabla \times \mathbf{f}(\mathbf{x}, t)}{v_s(\mathbf{x})^2 \rho(\mathbf{x})} \quad (2)$$

where  $\nabla \cdot$  is a divergence operator,  $\Delta$  is a Laplace operator,  $\nabla \times$  is a curl operator, and  $\mathbf{f}(\mathbf{x}, t)$  is a vector force density or seismic source term. Using Helmholtz decomposition, the source term can be decomposed into two parts (Muller, 2007),  $\mathbf{f} = \mathbf{f}_p + \mathbf{f}_s$ , a curl-free and divergence-free,  $\mathbf{f}_p$  and  $\mathbf{f}_s$  respectively, so that,

$$\nabla \cdot \mathbf{f} = \nabla \cdot \mathbf{f}_p = L \text{ with } \nabla \cdot \mathbf{f}_s = 0 \quad (3)$$

$$\nabla \times \mathbf{f} = \nabla \times \mathbf{f}_s = \mathbf{T} \text{ with } \nabla \times \mathbf{f}_p = 0. \quad (4)$$

In the passive seismic method, the goal is to identify the micro-seismic events, which are described by the source term,  $\mathbf{f}(\mathbf{x}, t)$ , by measuring the displacement,  $\mathbf{u}(\mathbf{x}, t)$ , on or below the Earth surface at a set of discrete points  $\{\mathbf{x}_r\}$ , the receiver locations. Therefore, only a subset of  $\mathbf{u}(\mathbf{x}, t)$  is known,  $\{\mathbf{u}(\mathbf{x}_r, t)\}$ .

If the velocity and density are given, the passive seismic imaging/inversion problem is linear; thus, following the geometrical optics theory, forward modeling operator (Aki and Richards, 2009), and adjoint operator, often called beamforming, diffraction stacking, or Kirchhoff operator (Johnson and Dudgeon, 1993; Duncan et al., 2010; Borcea et al., 2011), can be modified and, with a far-field displacement approximation, it is similar to Haldorsen et al. (2013) formulation:

$$L_{LSS}^M(\mathbf{x}, t) = \frac{v_p(\mathbf{x})^2 \rho(\mathbf{x})}{N} \sum_{r=1}^N \text{sign}_M^p A(\mathbf{x}_r, \mathbf{x}) \mathbf{u}(\mathbf{x}_r, t + \tau_p(\mathbf{x}_r, \mathbf{x})) \cdot \hat{\mathbf{r}}(\mathbf{x}_r, \mathbf{x}) \quad (5)$$

$$\mathbf{T}_{LSS}^M(\mathbf{x}, t) = \frac{v_s^2(\mathbf{x}) \rho(\mathbf{x})}{N} \sum_{r=1}^N \text{sign}_M^s B(\mathbf{x}_r, \mathbf{x}) \mathbf{u}(\mathbf{x}_r, t + \tau_s(\mathbf{x}_r, \mathbf{x})) \times \hat{\mathbf{r}}(\mathbf{x}_r, \mathbf{x}) \quad (6)$$

where  $N$  is the number of receivers,  $\text{sign}_M^{p/s}$  are the moment tensor polarity corrections for P and S waves (Thornton and Eisner, 2011),  $\tau(\mathbf{x}_r, \mathbf{x})$  is travel-time from receiver location  $\mathbf{x}_r$  to a given point in space  $\mathbf{x}$ ,  $A$  and  $B$  provide a positive weights to compensate for changes of amplitude due to wave propagation, such as, spherical divergence and absorption, and  $\hat{\mathbf{r}}$  is a unit ray vector at location  $\mathbf{x}$  from the source location  $\mathbf{x}_r$ .

The divergence-free part of source wavefield,  $\mathbf{T}$ , can be further decomposed into two parts:  $\mathbf{T} = \mathbf{T}_h + \mathbf{T}_v$ , one within the horizontal and the other within the vertical plane and both perpendicular to the direction of the wave propagation. The magnitude of the divergence-free source wavefield can be estimated as  $l_2$  norm:  $T = |\mathbf{T}| = \sqrt{\mathbf{T}_h^2 + \mathbf{T}_v^2}$ .

Finally, we can use the components to create a *seismic image*  $i(\mathbf{x})$  which can be identified as a correlation of RMS integral

## Passive seismic multicomponent imaging using geometrical optics theory

of  $L$  and  $T$  wavefields over a time period  $\Delta t_p$  and  $\Delta t_s$ , respectively:

$$i(\mathbf{x})_{t_i} = i(\mathbf{x})_{t_i}^L * i(\mathbf{x})_{t_i}^T$$

$$= \sqrt{\frac{1}{\Delta t_p} \int_{t_i+\Delta t_p} L(\mathbf{x}, t)^2 dt} * \sqrt{\frac{1}{\Delta t_s} \int_{t_i+\Delta t_s} T(\mathbf{x}, t)^2 dt} \quad (7)$$

where  $\Delta t_p$  and  $\Delta t_s$  are taken to be equal to duration of P and S wavelets. The seismic image can be considered to be a local maximum likelihood estimator of the passive event location (Garnier, 2011). Therefore the estimated origin time,  $t_0$ , and estimated location,  $\mathbf{x}_{img}$ , of passive seismic event are given as:

$$t_0 = \arg \max_{t_i} i(\mathbf{x})_{t_i}; \mathbf{x}_{img} = \arg \max_{\mathbf{x}} i(\mathbf{x})_{t_0} \quad (8)$$

### SYNTHETIC EXAMPLE

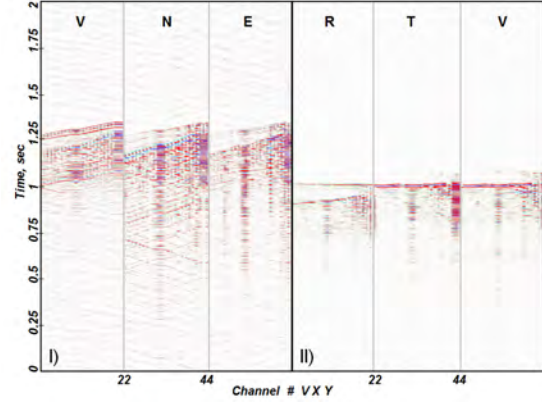
In the noise-free synthetic example, a downhole seismic acquisition is used, containing 16 3-C receivers 15 meters apart, Figure 1. The  $v_p$  and  $v_s$  velocities are assumed to be given and constant,  $v_p = 3400 \frac{m}{s}$ ,  $v_s = 2300 \frac{m}{s}$ . The seismic source is a point source radiator multiplied by a moment tensor  $M$ , corresponding to a double-couple source with strike, dip, and rake of (45,60,90) at location  $\mathbf{x}_0 = (150m, 100m, 150m)$  relative to the middle of the array, Figure 1.

In the synthetic example, where we used geometrical optics theory based modeling (Aki and Richards, 2009), first, we will demonstrate all the steps we apply to raw data in order to achieve the suggested imaging, as shown on Figure 2.

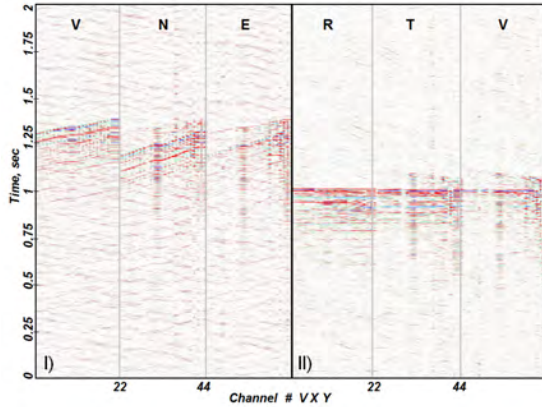
### Implementation steps

First, the seismic raw data are recorded (Figure 2a) on the 3-C downhole geophones in the downhole monitoring well. The 3-C geophones usually are not properly oriented, so a certain transformation is needed to be applied to raw data so that they represent data acquired from true/grid North East directions (Figure 2b). The oriented data,  $\{\mathbf{u}(\mathbf{x}_r, t)\}$ , are input to migration as explained in the theory section. This transformation is performed by using a known microseismic event location such as string shot or perforation shot.

Now, the data are ready for migration. To estimate the value of the passive seismic image at location in the subsurface  $\mathbf{x} - i(\mathbf{x})$ , we should follow equations 5 and 6: first we apply "rotations", that is, we calculate dot and vector products of data with direction vector,  $\hat{\mathbf{r}}$ , from a location of the subsurface,  $\mathbf{x}$ , to receiver location,  $\mathbf{x}_r$ , thus we create a radial (P) component from the dot product and magnitudes of two mutually perpendicular components, namely horizontal (SH) and vertical (SV), from the vector product (Figure 2c). Next, we apply a travel-time moveout, for given  $v_p$  and  $v_s$ , depending on the components (Figure 2d). At this point, we should apply spherical divergence, absorption, and moment tensor polarity corrections following equations 5 and 6. Finally, we stack separately each component and scale by appropriate scalars to get curl-free,  $L(\mathbf{x}, t)$ , and divergence-free,  $|\mathbf{T}_h(\mathbf{x}, t)|$  and  $|\mathbf{T}_v(\mathbf{x}, t)|$ , components, related to the source function,  $\mathbf{f}(\mathbf{x}, t)$ .



(a) Hydraulic fracturing signal



(b) Perforation shot

Figure 3: Field data examples: Two second windows of (a) hydraulic fracturing event and (b) perforation shot record. I - data oriented to true vertical, north, and east components. II - data rotated to radial, transverse, and vertical with moveout from its (a) imaged or (b) reported location on radial, transverse, and vertical components

If a potential source location  $\mathbf{x}$  is not close to the actual source location  $\mathbf{x}_0$ , first, the rotations are not adequate - do not enhance signal, and, second, the alignment of the signals are not achieved - the stacked value is not maximized. Therefore, only if  $\mathbf{x} = \mathbf{x}_0$  are both conditions fulfilled, suggesting that maximum value of the image represents the location of the microseismic event.

### Imaging results

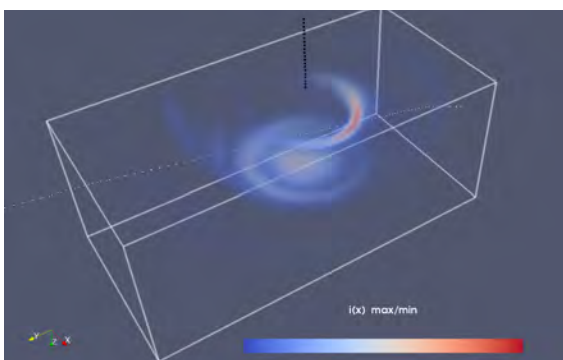
First, we create separate images for longitudinal,  $i(\mathbf{x})_{t_0}^L$ , and transverse,  $i(\mathbf{x})_{t_0}^T$ , parts of the source wavefield at origin time  $t_0$  (Figure 1(a)). Individually, these images show very large uncertainties, in the case of this one well downhole array. However, by combining the two components, by equation 7, the created passive seismic image,  $i(\mathbf{x})_{t_0}$ , manifests better constrained maximum, and thus, represents a less uncertain estimator of the event location (Figure 1(b) right). The image at origin time achieves maximum, which matches the true loca-

## Passive seismic multicomponent imaging using geometrical optics theory

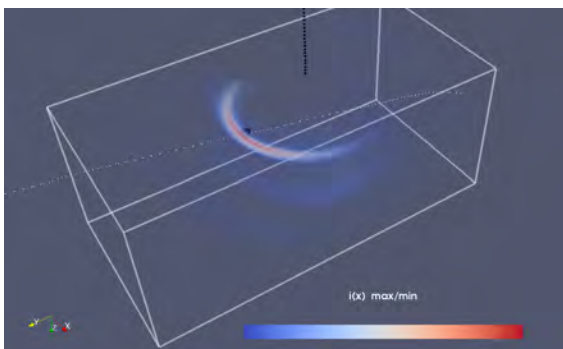
tion of the synthetic event.

As expected, the lack of aperture and the orientation of the array result in a rather large uncertainty of location estimation in azimuthal direction, while in depth and in radial direction the location estimation is better constrained and less uncertain.

However, in addition, we created the stacked image along all times,  $\sum_{t_i} i(\mathbf{x})_{t_i}$ , reflecting the significant uncertainty of the location estimator along the radial direction as well (Figure 1(b) left).



(a) Hydraulic fracturing event image



(b) Perforation shot image

Figure 4: Seismic images of (a) hydraulic fracturing event and (b) perforation shot with a monitoring well - black vertical dots, treatment well - white horizontal dots, and reported per-shot location - black large dot

### FIELD DATA EXAMPLE

In this example, both hydraulic fracturing and perforation shot events are recorded with a downhole acquisition system with 22 levels of 3-C geophones in the vertical monitoring well (Figure 3)

Figure 3 shows the way to perform quality control (QC) of the procedure, which is usually applied on field data. Recalling the facts stated in the synthetic case, the closer the imaging location is to actual seismic event location,  $\mathbf{x} \approx \mathbf{x}_0$ , the more enhancement in the rotation of the signals and the better alignment of the traces should be, thus, maximizing the components image values, created by the stacking.

In the example, the microseismic event, Figure 3 shows significant enhancement by rotation and splitting P and S energies on to radial (P), horizontal (SH), and vertical (SV) components, Figure 3(a). In addition, after applying travel-time moveouts the signals are aligned, maximizing the stack. The rotations and alignments are performed from the estimated location, based on picking maximum location from created seismic image, Figure 4(a). The QC procedure suggest that the estimated location is well defined.

On the other hand, the raw perforation shot signal, which location is known and usually used for velocity calibration, is much weaker comparing to the hydraulic fracturing event signal, Figure 3(b) I, which is seen on Vertical, North, and East components. However the same signal rotated to RTV grid and moved out from the known location demonstrates similar improvement in SNR as in the hydraulic fracturing microseismic event. Of course, stacking the traces of each components improves SNR. The QC for the perforation shots is that the imaged location is very close to the reported location (black dot on Figure 4(b)).

As we mentioned, the seismic images are created for these two microseismic events, as seen in Figure 4. On the figures, the presented seismic image contains the maximum value,  $i(\mathbf{x})_{t_0}$ , for a half of the second time window analyzed here. The maximum values are achieved close to the treatment well (white dots). The location of the maximum is the most probable position where the analyzed event occurred. The shape of maximum suggests the uncertainty of the estimation and, as shown in synthetic data, it is very large in the azimuthal direction relative to a downhole array.

### CONCLUSIONS

The described method of passive seismic imaging is a Kirchhoff type imaging applied to isotropic elastic wave equation. The source function is decomposed to divergence-free and curl-free components. These components are utilized to produce the passive seismic image.

The method was tested and found effective with a synthetic example: the maximum value of the seismic image matches exactly the location of the synthetic event in a noise-free environment. The synthetic example showed that the largest uncertainty is in azimuthal direction relative to given single vertical downhole array.

In a real data example, the imaging method successfully located a hydraulic fracturing event and the perf shot at a know location in the treatment well.

### ACKNOWLEDGEMENTS

The authors thank MicroSeismic, Inc. for permission to present this work.

## Passive seismic multicomponent imaging using geometrical optics theory

### REFERENCES

- Aki, K., and Richards, P.G., 2009, *Quantitative Seismology*, Second Edition, University Science Book
- Artman, B., Podladtchikov, I., Witten, B., 2010, Source location using time-reverse imaging, *Geophysical Prospecting*, 58, 861-873
- Borcea, L., G. Papanicolau, C. Tsogka, 2003, Theory and applications of time reversal and interferometric imaging, *Inverse Problem*, 19, 2003, S139-S164
- Duncan, P., and L. Eisner, 2010, Reservoir characterization using surface microseismic monitoring. *Geophysics*, 75(5), A139-A146
- Duncan, P., Lakings, D., Fores, R., 2010, Method for Passive Seismic Emission Tomography, 7663970 B2, Feb. 16, 2010, MicroSeismic Inc.
- Drew, J., Leslie, P. Armstrong, G. Michaud, 2005, Automated microseismic event detection and location by continuous spatial mapping: Annual Technical Conference and Exhibition, SPE 95513.
- Fuller, B., Engelbrecht, L., Van Dok, R., Starling, M., Diffraction processing of downhole passivemonitoring data to image hydrofracture locations, SEG Technical Program Expanded Abstracts 2007: 1297-1301.
- Garnier, J., 2011, *Imaging in Random Media*, Gene Golub SIAM Summer School: Waves and Imaging, University of British Columbia, Vancouver, Canada. <http://www.siam.org/students/g2s3/2011/random.html>
- Geiger, L., 1912, Probability method for the determination of earthquake epicenters from the arrival time only: *Bulletin of St. Louis University*, 8, 60-71
- Haldorsen, J., Brooks, N., Milenkovic, M., 2013, Locating microseismic sources using migration-based deconvolution. *Geophysics*, 78(5), 78KS73-78KS84
- Johnson, H.D., and E.D. Dudgeon, 1993, *Array signal processing, concepts and techniques*, Prentice Hall
- Muller, G., 2007, *Theory of Elastic Waves*, University of Hamburg, Samizdat Press, <http://samizdat.mines.edu/muller/>
- Shearer, P., 2009, *Introduction to Seismology*, Second Edition, Cambridge University Press
- Thornton, M., and L. Eisner, 2011, Method for passive seismic emission tomography including polarization correction for source mechanism, US Patent 7978563, July 12 2011, MicroSeismic Inc.